Materials & Design 239 (2024) 112800

Contents lists available at ScienceDirect

Materials & Design

journal homepage: www.elsevier.com/locate/matdes

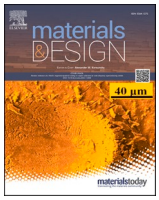

Silver nanoparticle coatings with adjustable extinction spectra produced with liquid flame spray, and their role in photocatalytic enhancement of TiO_2

Miika Sorvali [a], Tuomas Tinus [b], Jerin Thamby [c], Mari Honkanen [d], Harri Ali-Löytty [b,e], Alireza Charmforoushan [a], Mika Valden [b], Jarkko J. Saarinen [c], Jyrki M. Mäkelä [a,*]

[a] Aerosol Physics Laboratory, Physics Unit, Faculty of Engineering and Natural Sciences, Tampere University, P.O. Box 692, FI-33014 Tampere, Finland
[b] Surface Science Group, Physics Unit, Faculty of Engineering and Natural Sciences, Tampere University, P.O. Box 692, FI-33014 Tampere, Finland
[c] Department of Chemistry, University of Eastern Finland, Joensuu FI-80101, Finland
[d] Tampere Microscopy Center, Tampere University, FI-33014 Tampere, Finland
[e] Liquid Sun Ltd., Tekniikankatu 1, FI-33720 Tampere, Finland

A B S T R A C T

Silver nanoparticles deposits were produced with liquid flame spray (LFS) on glass and TiO_2 substrates to study their optical response and photocatalytic enhancement. The correlation between extinction spectrum of the nanoparticle coating and the LFS process parameters was studied. The spectra consisted of two partly overlapping peaks: one centered in the UV region and the other in the visible light region. The visible light peak redshifted as either the silver mass concentration in the precursor solution or the precursor solution feed rate was increased, which also correlated with growing primary particle size. However, simultaneous correlation with photocatalytic activity of the decorated TiO_2 surfaces was not observed, which was attributed to particle sintering on the surface. Instead, the photocatalytic activity was seen to change as the surface coverage of silver nanoparticles was varied. When the surface coverage was raised from ~10 % to roughly 30 %, the activity, and then decreased as the loading was further raised. The increase was assumed to originate from plasmonic activation, and the decrease was attributed to the excessive amount of silver either blocking reactive area of the TiO_2 or absorbing/scattering too much of the incoming light, which hindered the photocatalytic activity.

1. Introduction

Metallic nanoparticles have unique optical properties that can be exploited in various applications. Especially gold and silver nanoparticles have been utilized in photocatalysts, as their plasmonic activity enhances the photocatalytic activity in the UV region, and can expand the activity to visible light, and even near infrared (NIR) region [1–5]. Small individual silver particles are mostly plasmonically active in the UV region, but for dimers and larger particles, plasmonic activity extends towards longer wavelengths [6]. Broader range of electromagnetic radiation can potentially be utilized with a wider range of particle sizes and morphologies [5]. The plasmonic properties also depend on interparticle coupling, which emphasizes the importance of structural design of photocatalytic systems. These effects come into play with particle agglomeration and deposition on a substrate when the distance between individual particles becomes short enough [5–10]. As a consequence, nanoparticle loading can have a significant effect on the absorption-to-scattering ratio in plasmonic nanoparticle coatings [5]. Affecting the absorption is of particular interest in photocatalytic applications, where incorporation of plasmonic nanoparticles with TiO_2 photocatalyst has proven a viable method to extend the absorption to the visible light region of solar spectrum [11].

Temerov et al. [3] prepared photocatalytic inverse opal structures of TiO_2, and used Liquid Flame Spray (LFS) to coat the structures with silver nanoparticles. The nanoparticle addition was observed to clearly enhance the photocatalytic degradation of acetylene and splitting of water vapor under simulated sun light, which was attributed to the surface plasmon resonance (SPR) effects of Ag nanoparticles [12]. The LFS parameters were, however, not optimized, which left a lot of development for the structural design of the system. Furthermore, silver nitrate/water solution used in the study has been observed to combust inefficiently in the flame, which results in plenty of wasted precursor, and calls for improvement of the synthesis process, as more economic and ecological processes are increasingly required. Gogoi et al. [13] and Mogal et al. [14] have also succeeded in preparing Ag-covered TiO_2 structures exhibiting enhanced photocatalytic activity.

LFS is a particular flame spray pyrolysis method that can be used for producing metal and metal oxide nanoparticles and nanoparticle

* Corresponding author.

https://doi.org/10.1016/j.matdes.2024.112800
Received 30 November 2023; Received in revised form 16 February 2024; Accepted 24 February 2024
Available online 25 February 2024

coatings [15,16]. In the LFS process, either oxygen or hydrogen is used to atomize a liquid jet of precursor solution into a turbulent H_2/O_2 flame, where the droplets combust and nanoparticles are formed via various aerosol processes. The allure of using LFS in this kind of an application is the simplicity, the inexpensiveness, and the speed and continuousness of the process. This could enable efficient and scalable production of photocatalysts in the future. Therefore, studying how the plasmonic response can be tuned by adjusting the process parameters, and figuring out how to optimize silver nanoparticles for photocatalytic applications, is vital for the upcoming studies.

As the interaction between light and silver nanoparticles has an essential role in enhancing photocatalytic activity through plasmonic coupling, UV–Vis measurements of the LFS-produced silver particles is a good first point of contact for characterizing their plasmonic activity [5]. This study consists of two parts. Firstly, we explored how the extinction spectrum of LFS-made silver nanoparticle deposits could be tuned using just plain soda-lime glass slides as substrates. In the second part, we changed the substrates to planar TiO_2 thin film photocatalysts prepared by Atomic Layer Deposition (ALD) and studied what governs the photocatalytic enhancement caused by the silver particle deposits. Once the understanding of photocatalytic enhancement through adjusting the LFS parameters is achieved on a planar substrate, this knowledge can hopefully be transferred to more complex substrates like inverse opals, and utilized by scientists working in the field.

2. Materials and methods

2.1. Synthesis of Ag nanoparticle coatings

The first step of the study was producing a set of silver nanoparticle coatings on soda-lime glass slides with different LFS parameter combinations. In the LFS coating process, oxygen was used as the atomizing gas, hydrogen as the fuel gas, and an inert nitrogen flow in between the oxygen and hydrogen flows to adjust the spatial position where the combustion starts. The coating setup and the structure of the burner is described in Fig. 1. The glass substrates were passed over the flame a certain number of times (referred to as coating cycles) to deposit a controlled amount of silver nanoparticles. The fixed parameters for all depositions were the O_2 flow rate of 10 slpm (standard liters per minute), the N_2 flow rate of 5 slpm, and the deposition height of 20 cm above the burner. A more comprehensive description of the LFS process in general can be found in the literature [15–17]. The burner model used here has been referred to as “KP burner” in the earlier studies.

The chemicals used for the precursor solutions were silver nitrate ($AgNO_3$), 99.9+%, Alfa Aesar), acetone (AnalaR NORMAPUR, VWR) and deionized water. The precursor solution was varied by adjusting the silver mass concentration ($C_{M,Ag}$) (100, 225, 350 or 475 mg/ml) and the solvent composition. One set of samples was prepared with each different silver concentration and a fixed water-to-acetone volume ratio of 65:35. Additional solvent ratios were also used for varying concentrations based on the solubility of silver nitrate into the water/acetone mixture (50:50 for 350 mg/ml, 35:65 for 225 mg/ml and 20:80 for 100 mg/ml), since lower silver concentrations allowed for higher acetone fractions, while still maintaining complete dissolution. By replacing part of the water with acetone, combustion enthalpy was raised, thereby enhancing the combustion. The precursor solution was fed into the flame at a rate (Q_l) of 2, 4 or 5.5 ml/min, and the H_2 gas flow rate (Q_{H2}) was set to either 20 or 35 slpm. The number of coating cycles (N_C) was determined for each parameter combination by calculating a theoretical silver deposition amount ($C_{M,Ag} \cdot Q_l \cdot N_C$). This value was adjusted as close to a fixed value for each samples by changing N_C, which would theoretically transfer to comparable masses of silver on the surface. However, some variation in the actual deposited amount is bound to form due to probable differences in particle flux and deposition rates based on each parameter combination.

Based on the results gained from the first sample set, certain parameter combinations ($C_{M,Ag}$, Q_l, Q_{H2}, N_C) were selected for the second part of the study focusing on photocatalytic activity enhancement. For these samples, the substrates were fused quartz microscope slides that were coated with a 30 nm thin film of anatase TiO_2 photocatalyst by ALD. The LFS coatings were performed on these TiO_2/quartz substrates similarly than on the bare soda-lime glass slides.

2.2. Fabrication of TiO_2 photocatalyst thin films

The TiO_2 thin films were fabricated with a Picosun Sunale ALD R200 Advanced reactor at the growth temperature of 175 °C using the process described in detail by Saari et al. [19]. The layers were deposited on thermally stable fused quartz microscope slides (UQG Optics). The 30 nm thickness of the thin film was determined by ellipsometry (Rudolph Auto EL III Ellipsometer, Rudolph Research Analytical, $\lambda = 632.8$ nm). This corresponded to 634 coating cycles, which results in a growth-per-cycle rate of 0.0473 nm/cycle. After the deposition, the samples were annealed in air in a tube furnace (Carbolite Gero) at 500 °C for 1 h to induce complete crystallization to anatase [20].

2.3. Sample characterization

UV–Vis measurements were performed on the soda-lime glass samples with a Cary 60 UV–Vis Spectrophotometer, measuring extinction spectra from 300 to 800 nm. The spectrum of a clean glass slide was first measured as a reference, which was then subtracted from the spectra measured for the Ag-coated slides. Transmission Electron Microscope (TEM) samples were prepared on TEM grids alongside the glass slide samples using otherwise the same synthesis parameters, but with reduced N_C to minimize the number of overlapping particles. The samples were imaged with JEOL JEM-F200 TEM, and ImageJ was used to calculate particle size distributions from the TEM micrographs. The program calculated particle area distributions from several micrographs using suitable thresholding. The area distributions were then transformed into diameter distributions by assuming spherical particle shape for all particles. Particles smaller than 5 nm in diameter were omitted in the automatic detection, because using a very low threshold can lead to inclusion of darker areas without any actual particles. Particles down to

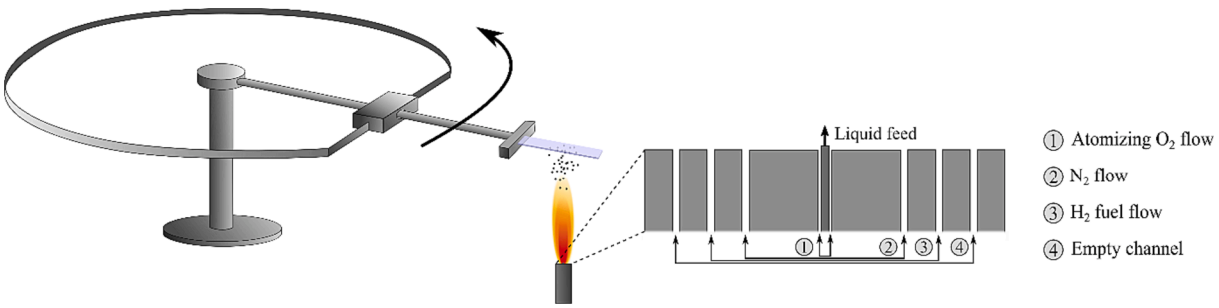

Fig. 1. A scheme of the coating process, and the structure of the burner and the gas flow configuration used. Adapted from Sorvali et al. [18].

ca. 2 nm diameter could, however, be visually discerned, and these ultrafine (<5 nm) particles were manually counted from the images and added to the total distributions as a size bracket of particles 0–5 nm. This approach was assumed relatively reliable for determining size distributions, because the fraction of particles clearly consisting of more than one primary particle was counted from the TEM images to be between 5 and 9 % of the total particle number in every sample. Possible bias in some direction can originate from the particle deposition process onto the TEM grids. Samples with several coating cycles used in the photocatalytic activity measurements were imaged with a Scanning Electron Microscope (SEM, Zeiss UltraPlus FE-SEM), using an additional 5 nm carbon coating to avoid surface charging.

2.4. Photocatalytic activity measurements

The photocatalytic activity was characterized by gas-phase photooxidation of acetylene (C_2H_2) into CO_2 and H_2O in an in-house built reactor [21,22]. The samples were placed inside a reaction chamber which was filled with a regulated mixture of acetylene and technical air at a rate of 80 ml/min and 100 ml/min, respectively. The reaction chamber was then irradiated with a high intensity broad spectrum light source (XBO 450 W OFR from Osram, High Power Xenon Light Sources) through a quartz glass window, resulting in oxidation of acetylene into CO_2. The CO_2 produced was monitored in real time using a CO_2 sensor (Vaisala GMP343) and Vaisala MI70 transmitter, assisted with a temperature sensor (Thorlabs TSP01) and a pressure gauge (Wika PGT01).

Gaseous acetylene was selected as a test molecule for the photocatalytic activity due to its simple nature, and so that all mechanical stresses could be removed from the sample surface compared to typical liquid-phase test setups. The detailed reaction mechanisms have been described by Temerov et al. [3]. The increased activity was measured in the ppm level by using an optical CO_2 detector.

3. Results and discussion

Silver nanoparticle deposits on a clean soda-lime glass slides

Let us first examine the UV–Vis results measured from the soda-lime glass slides coated with silver nanoparticles. Fig. 2a shows extinction spectra representing each different precursor solution used. The presented spectra are average spectra calculated over all the samples prepared with that specific solution, and are therefore not equal to any single measured spectrum. The shape of the spectrum was, however, similar for most samples, and the measured extinction spectra for each individual sample can be found in the supplementary material organized in two different ways (Figs. S1 and S2). The silver mass concentration in the solution (mg/ml) is expressed as the first number in the legend, and the ratio in parentheses refers to the water-to-acetone volume ratio of the solvent mixture. Since the number of coating cycles could not be adjusted to set the theoretical deposited mass (described in the experimental section) exactly equal for all samples, the extinction intensities were scaled accordingly to level out the theoretical differences, so the spectra would be as comparable as well as possible. A clear bimodal nature was observed in almost all measured spectra, consisting of two partly overlapping peaks: one centered in the UV region and the other in the visible light region. Let us refer to the peak centered in the UV region as UV-Peak and to the peak centered in the visible light region as VIS-Peak. There are different features in the extinction spectra that can be examined, such as peak positions, peak intensities or integral spectral areas.

Clear correlations between the above-mentioned features and the synthesis parameters were difficult to draw. However, the peak positions seemed to best correlate with the parameters. Fig. 2b depicts the average VIS-Peak position as a function of silver mass concentration (blue stars and the lower x-axis) and precursor solution feed rate (red circles and the upper x-axis). The error bars signify the standard deviation among the samples prepared with a fixed Ag mass concentration or solution feed rate. The remark placed in Fig. 2b means that for the lowest concentration and solution feed rate, the average wavelength should in reality be lower and the error bar (standard deviation) should be larger. This was due to the VIS-Peak widening significantly and/or the two peaks overlapping too strongly for some samples to determine the VIS-Peak position, resulting in omission of the lowest position values in the calculations.

The VIS-Peak generally redshifted as either the concentration or the solution feed rate was increased, in other words, as the amount of silver in the flame zone was raised. Both factors likely resulted in larger particles and/or more agglomeration on the surface, which are known to move the scattering component in the extinction spectrum towards longer wavelengths in the visible range [6,23]. The concentration understandably had a larger effect, since increasing the solution feed rate

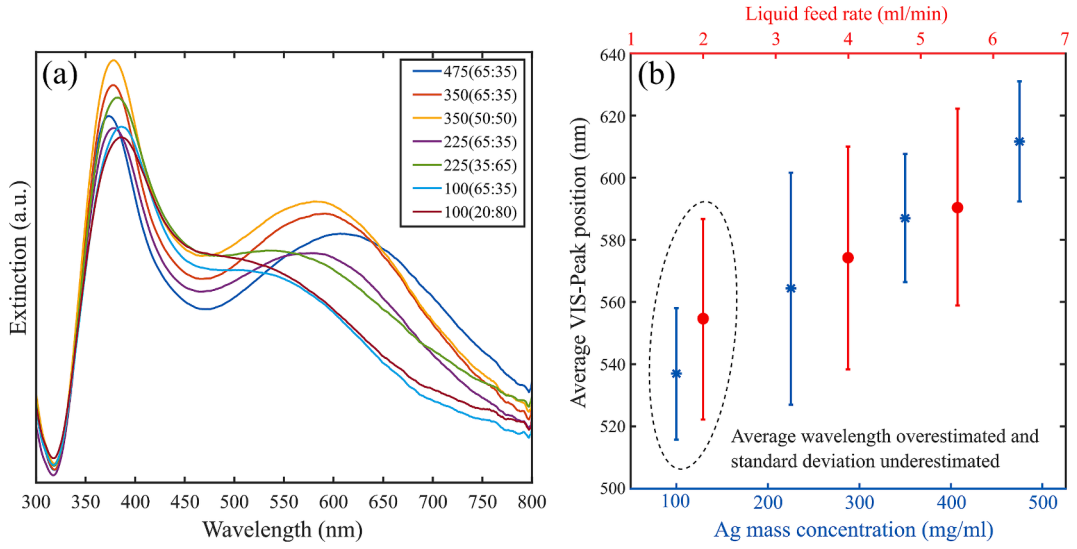

Fig. 2. (a) Extinction spectra for each precursor solution, averaged over all different samples produced with that specific solution. The legend indicates first the silver mass concentration in mg/ml, and in the parentheses the water-to-acetone volume ratio in the solution. (b) The average VIS-Peak position as a function of precursor solution feed rate and silver mass concentration. The error bar depicts the standard deviation between different samples produced with a certain concentration or feed rate.

also raises the volume of solvents in the flame. The redshift was often, but not always, accompanied with an increase in the VIS-Peak intensity (Fig. S1). The solvent composition did not seem to have a very significant effect on the averaged spectra. This could mean that already the lower 35 % fraction of acetone in the precursor solution was adequate to induce efficient combustion, so the addition from that only slightly raised the combustion enthalpy.

Another factor that was observed to correlate with increasing concentration was the decreasing standard deviation of the average VIS-Peak position. As there was more silver in the precursor solution, the effect of changing other parameters diminished. This is presumed to originate from the growing particle size. As the redshift of the VIS-Peak induced by the increasing primary particle size starts to dominate over the effect originating from agglomeration/stacking of the particles, changing other parameters, which are assumed to have an impact on the deposition of particles, seize to have as dramatic an effect on the shape of the spectrum. Conversely, agglomeration/stacking is assumed to have a more pronounced effect on the shape, when the average particle size is smaller.

The H_2 flow rate is an interesting parameter, as its effect seemed to be very dependent on the other parameters. Raising the flow rate from 20 to 35 slpm produced more variance between extinction spectra of the samples produced from different precursor solutions, which is clearly observable in Fig. S2. However, when the extinction spectra were averaged over all samples produced with 20 slpm and 35 slpm H_2 flow rates, the shapes of the average spectra for both flow rates turned out very similar (Fig. S3). This also notably reveals the only systematic effect of raising the flow rate: an increase in the total extinction intensity. This is probably due to enhanced particle deposition, which leads to a higher silver mass on the surface. Raising the H_2 flow rate stretches the flame, which results in the flame tip moving closer to the substrate when the coating distance from the burner is kept fixed. This creates a larger temperature gradient between the particles and the substrate. Since thermophoresis is generally considered the main mechanism of particle deposition from the flame [24–26], a higher total mass of silver on the surface would be expected. The higher variance between the samples with 35 slpm H_2 flow rate could also be affected by a more complex deposition behavior of the particles. Raising the temperature on the substrate surface during deposition also enhances particle sintering, which likely has an effect on the particle shape and size distribution, and therefore on the plasmonic properties. However, the effect of the substrate properties and the synthesis parameters to the deposition has not been systematically studied, and is therefore still not properly understood.

In addition to the VIS-Peak shift, an inverse correlation was observed for the UV-Peak. As the VIS-Peak redshifted, the UV-Peak simultaneously blueshifted. This correlation is depicted in Fig. 3.

This effect is believed to be caused by differences in the primary particle size distribution. It is generally assumed that very small separate silver particles are mainly plasmonically active in the UV region, so the blueshift could be connected to the ultrafine particle fraction. This effect is elaborated in the next section as the TEM images of the particles are examined.

3.1. TEM imaging of silver particles

TEM samples were prepared based on the UV–Vis measurements of the Ag-coated soda-lime glass slides with 5 specific parameter combinations that were picked to represent a wide range of different VIS-Peak positions and varying peak intensities. The parameters (TAg1-TAg5) are listed in Table 1 with an additional sample TAg6 that was used in other measurements and SEM imaging. The TEM samples were prepared with the same parameters as the UV–Vis samples, except N_C was reduced in every case.

The TEM samples were comprehensively imaged and several micrographs for each sample were used to count particles of different sizes.

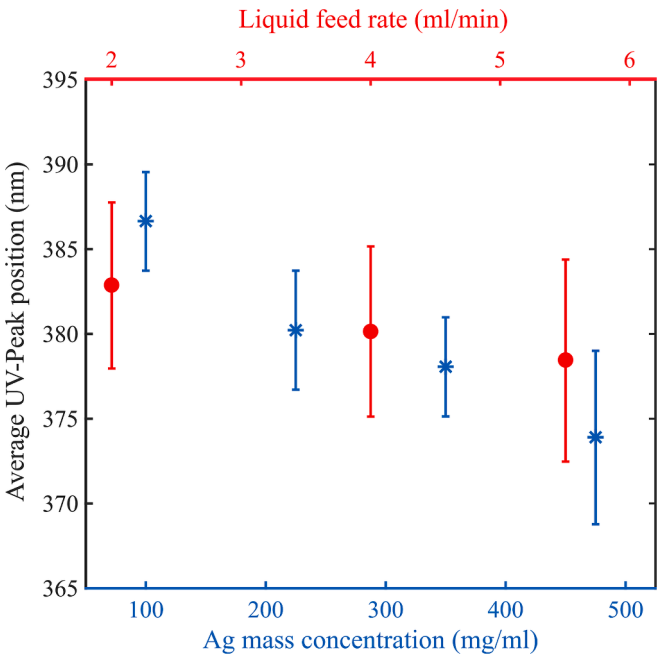

Fig. 3. The average UV-Peak position as a function of silver mass concentration (blue stars and bottom x-axis) and liquid feed rate (red circles and upper x-axis). (For interpretation of the references to colour in this figure legend, the reader is referred to the web version of this article.)

Table 1
Parameter combinations chosen for TEM imaging of Ag nanoparticles (TAg1-TAg5), plus an additional combination TAg6 that was used in later characterization.

Sample name	Concentration (mg/ml)	Water-to-acetone volume ratio	Hydrogen flow rate (slpm)	Liquid feed rate (ml/min)
TAg1	475	65:35	35	4
TAg2	225	65:35	35	4
TAg3	225	65:35	20	2
TAg4	100	65:35	20	6
TAg5	100	65:35	20	2
TAg6	100	20:80	35	6

Fig. 4 shows the extinction spectra for the samples TAg1-TAg5, and the number and mass size distributions calculated based on TEM image processing. The 0 – 5 nm size bar was counted manually from the images. Other bars are presented in 1 nm steps in particle diameter. The mass count distributions were calculated from the number count distributions to visualize where the mass of the produced silver is focused. Fig. 5 shows representative TEM images of the produced samples TAg1-TAg5, and the average VIS-Peak position as a function of number mean diameter and mass median diameter. All diameter values were calculated for particles larger than 5 nm that could automatically be discerned in the micrographs by ImageJ.

With the chosen samples, the size effect of the particles is reflected clearly in the position of the visible light peak. Both the mass median diameter and the number mean diameter fall very nicely on a straight line. Therefore, in these samples the agglomeration/stacking effect is not presumed to play a significant role for the extinction spectrum. Another notable observation is that the particles in the TEM samples seemed to be very individual rather than strongly agglomerated, contrary to what is usually expected in flame synthesis. This indicates that the agglomeration and sintering mainly happens on the substrate surface instead of in the gas phase, which was also observed in SEM images presented later.

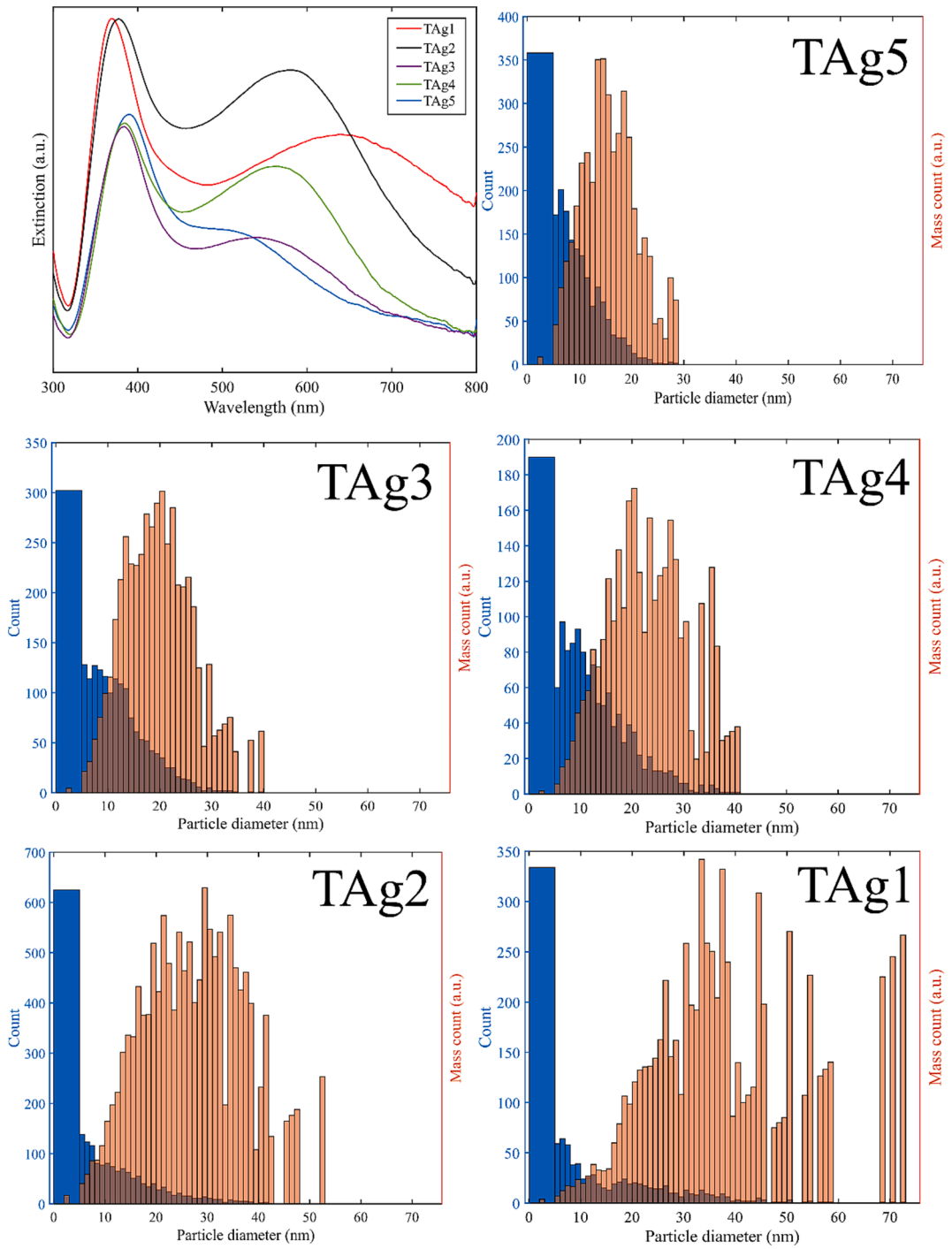

Fig. 4. The extinction spectra of the samples deposited on soda-lime glass and corresponding to the parameter combinations TAG1-TAg5, and the size and mass distributions from TEM samples prepared with corresponding parameter combinations but a lowered number of coating cycles. The distributions were counted from several TEM micrographs for each sample. The number count is drawn in blue and the mass count in orange. (For interpretation of the references to colour in this figure legend, the reader is referred to the web version of this article.)

As we concluded in the previous chapter, the VIS-Peak position correlated with two parameters: silver mass concentration and the precursor solution feed rate. Depending on the parameter combination, either of these can be the dominant factor for a specific sample. Sample TAg4 has a larger average particle size, and therefore a stronger VIS-Peak redshift compared to sample TAg3, although TAg3 has a higher mass concentration (and H_2 flow rate). On the other hand, the higher solution feed rate of TAg4 seems to override the effect of higher concentration of TAg3 in this case. These two factors seem to have quite a similar effect on the particle size distribution, and therefore the VIS-Peak redshift. It seems that increasing the feed rate of silver into the flame, no matter through which parameter adjustment, is the key for inducing a redshift of the VIS-Peak in the extinction spectrum.

In the size distributions in Fig. 4, we can see how the average particle size shifts towards larger particles as the VIS-Peak redshifts. However, in all samples there is a fraction of ultrafine particles under 5 nm in diameter. This is believed to be connected to the blueshift of the UV-Peak that happens simultaneously with the redshift of the VIS-Peak,

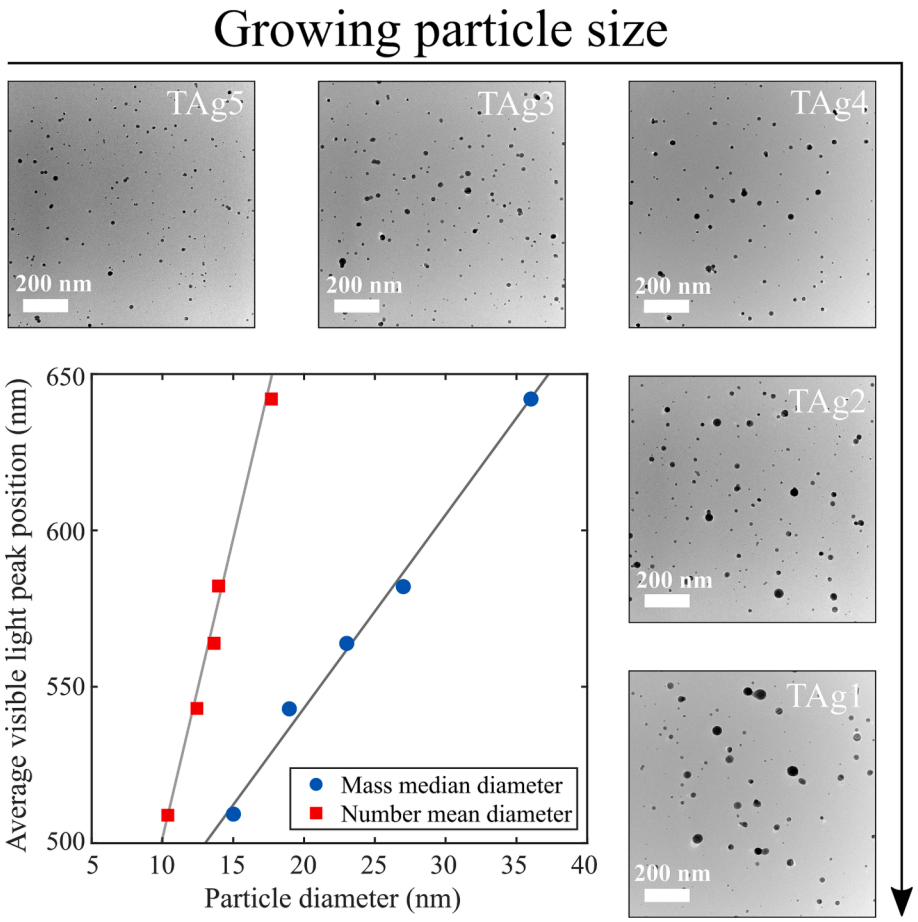

Fig. 5. The average VIS-Peak position as a function of number mean diameter and the mass median diameter for particles larger than 5 nm in diameter. Around the graph, representative TEM images of samples corresponding to parameter combinations TAg1-TAg5 are presented.

mentioned in the previous section. While the ultrafine particle mode seems to be present in every sample, the size fraction of 5–10 nm diminishes when the average size increases. This results in the ultrafine mode being more prevalent in the part of the particle distribution under 10 nm in diameter. Since the UV-Peak position blueshifts with decreasing Ag nanoparticle size, the blueshift can be expected as the mean particle size of the 0–10 nm fraction decreases [27].

3.2. Photocatalytic activity of the Ag-coated TiO2 substrates

Now we move on to the second part of the study. All the samples studied in this part were planar TiO_2 thin films on quartz glass slides that were coated with Ag nanoparticles. The photocatalytic activities for the parameter combinations TAg1-TAg6 were measured to study if the synthesis parameters, the extinction spectra, and the particle size distributions could be coupled with the photocatalytic enhancement of the TiO_2 thin film. Samples for each parameter combination were prepared using two different silver loadings controlled by N_C (referred to as "Low cycles" samples and "High cycles" samples). The "High cycles" samples were prepared with identical parameter combinations (TAg1-TAg6) and N_C to the samples deposited on the soda-lime glass slides, but for the "Low cycles" samples N_C was dropped to one third to induce a difference in the silver loading on the surface. The exact number of coating cycles used for each sample is listed in Table 2.

An additional set of samples, "Varying cycles", was prepared to study the effect of silver loading on the photocatalytic activity in more detail. For these samples, the parameter combination TAg6 was picked and N_C was varied between 1 and 8. The photocatalytic activities measured for the "Varying cycles" samples are presented in Fig. 6.

Table 2
The number of silver coating cycles for "low cycles" and "high cycles" samples. All of these samples were prepared on TiO_2 thin films.

	TAg1	TAg2	TAg3	TAg4	TAg5	TAg6
Low cycles	1	2	4	3	8	3
High cycles	3	6	12	8	24	8

Excluding one sample, all measurements gave an enhancement in the photocatalytic activity of up to 30 %. Using the same photocatalytic test and similar LFS Ag nanoparticles synthesis but on three-dimensional inverse opal TiO_2 structure, Temerov et al. [3] also observed Ag nanoparticles to improve photocatalytic activity. The use of thin film photocatalyst here allows us to discuss the optimization of the LFS parameters without the added complexity of substrate morphology.

The parameter combinations TAg1-TAg5 were chosen based on their varying redshifts of the VIS-Peak in the extinction spectrum. Even though this correlated well with the average particle size, no such clear correlation was found with the photocatalytic enhancement. Conversely, the activity values seemed to vary quite randomly among the different samples. This could at least partly be connected to particle sintering on the titania surface, which creates a disconnect between the results obtained from the soda-lime glass samples and the TiO_2 samples. Surprisingly, the "Low cycles" samples systematically produced higher photocatalytic activities compared to the "High cycles" samples. This suggests that the silver loading could be more a relevant factor to the photocatalytic enhancement than the particle size distribution.

Fig. 6b expresses behavior where the activity rises when silver particles are introduced on the TiO_2 surface, reaches a maximum value at

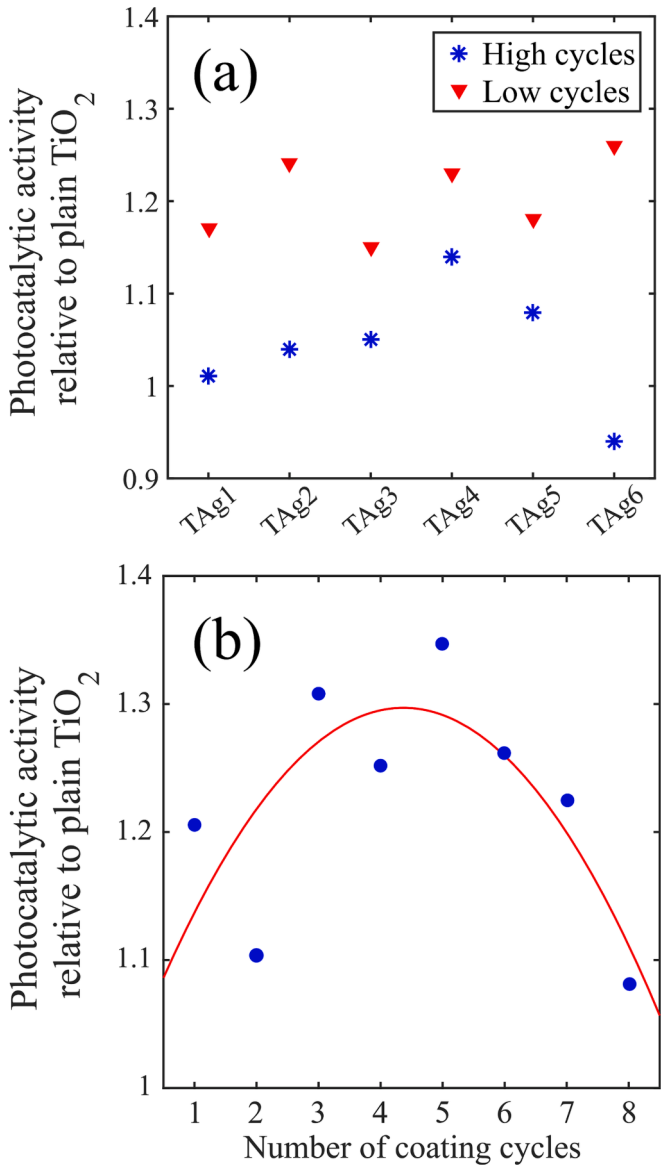

Fig. 6. Photocatalytic activities of (a) the "High cycles" samples and "Low cycles" samples, and (b) the "Varying cycles" samples. All activities are presented as relative values to a TiO_2-coated quartz glass without silver particle deposition.

around 4 to 5 coating cycles, and then decreases. The initial increase is explained by the plasmonic coupling mechanisms explained in detail by Temerov et al. [3]. Cushing et al. [28] have shown that for Ag/TiO_2 catalysts both plasmon-induced resonance energy transfer (PIRET) and hot electron injection processes contribute to the improved photocatalytic activity. In PIRET, energy is transferred non-radiatively from Ag nanoparticle to excite an electron-hole pair in TiO_2, while in hot electron injection an electron from the conduction band of the Ag nanoparticle is injected into the conduction band of TiO_2.[28,29]. Formation of a strong plasmonic field at the Ag/TiO2 interface, as well as suppression of charge carrier recombination via spatial separation of charges, were thought to further enhance the photocatalytic activity [3].

For the following decrease, we propose two possible mechanisms: (1) either the high amount of silver starts to block too much of the active reaction area of the TiO_2 surface, or (2) the silver absorbs or scatters too much of the incoming light, limiting the photocatalytic activation of the TiO_2 surface. In both cases, the plasmonic enhancement caused by the silver particles gets overridden by this blocking effect. If the particle size is a secondary factor to the silver loading for photocatalytic enhancement, lower concentrations could possibly be used to optimize the coating structure in the future study by carefully adjusting the silver loading.

Another approach to tackle the visible light activation of photocatalysts that has been developed is through doping of TiO_2 with a metal cation instead of our approach of coating the structure with another material. For example, Inturi et al. [30,31] and Sun et al. [32] have prepared Cr-doped TiO_2 photocatalysts by various methods, including flame synthesis, resulting in visible-light-active photocatalysts for gas-phase degradation of acetone and liquid-phase degradation of 4-chlorophenol. In this case, the activation was the result of incorporation of Cr^{+6} ions into the system that allow for a visible light active transition. Chambers et al. [33] have also doped TiO_2 with silver ions, thereby lowering the band gap and inducing antibacterial properties under visible light irradiation.

Even though the extinction spectra and the particle size distribution could not be properly linked to the photocatalytic activity, certain properties were observed to correlate with it. When the peak intensities and the integral areas (graphical integration) in the measured extinction spectra of "Low cycles" samples were inspected for the UV region (300–400 nm) and the visible light region (400–800 nm), the ratio of these two regions was seen to have a correlation with the activities. The "High cycles" samples were deemed unsuitable for this inspection, since the excessive silver loading was expected to nullify these correlations. Fig. S4 shows that photocatalytic activity tended to rise when the integral area of the visible light region in relation to the UV region increased. Similarly, the activity increased as the ratio of the VIS-Peak intensity to the UV-Peak intensity increased. Once a suitable silver loading is found, these kind of measures could possibly be used to probe the extinction spectra for finding optimal synthesis parameters without thorough sample analysis. However, these correlations are bit speculative, because we are comparing samples produced on two different substrates with similar LFS parameters, and we can not be sure it the properties directly translate from one substrate to another.

3.3. SEM imaging

We were also interested in the surface structure of the prepared silver coatings, and how the actual deposition relates to the photocatalytic activity. The "Low cycles" samples and the "Varying cycles" samples were imaged with SEM to see how the particle deposits differ from each other, and how the surface structure relates to the photocatalytic enhancement. The surface coverage of silver particles for each sample was determined from the SEM micrographs using ImageJ with suitable thresholding. The values were calculated as averages of several SEM images for each sample. Fig. 7 shows the photocatalytic activity of the samples as a function of surface coverage along with representative SEM images of a few selected samples. The "High cycles" samples were not imaged, so they could not be implemented in the results.

The results from "Low cycles" and "Varying cycles" samples fit well together. It seems that if the surface coverage is roughly over 10 %, the photocatalytic activity increases as the coverage is raised. The activity peaks at around 30 % and then starts to go down. The one data point ("Varying cycles" sample with 1 coating cycle) with the surface coverage value of around 8 % leaves some open questions, since it strays significantly from the fit representing the rest of the data. Since it is the only data point with under 10 % surface coverage, no conclusions can be made on how the photocatalytic activity behaves with very low silver particle loadings, or if the data point is just erroneous for some reason. This should be studied further in future work by lowering the silver concentration in the precursor solution, thus producing lighter silver loadings.

Slight differences were observed in the particle sizes between the different "Low cycles" samples, which are represented as SEM images in Fig. S5. But as the earlier results suggested, the particle size distribution

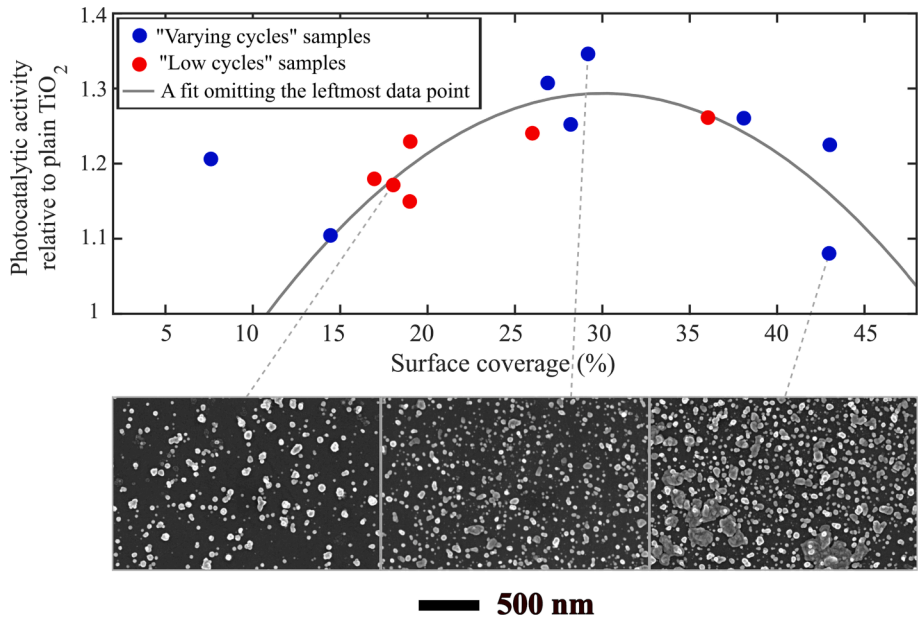

Fig. 7. Photocatalytic activity as a function of silver particle surface coverage. SEM images of "Low cycles" sample TAg1, "Varying cycles" sample with 5 coating cycles, and "Varying cycles" sample with 8 coating cycles, from left to right.

might not have that significant of an effect on the photocatalytic activity. However, as N_C is increased, the interaction between the flame and the surface starts to fuse the silver particles together, causing them to coagulate and form larger particles. At high N_C, we start to see larger sintered islands of silver shown in the rightmost SEM image of Fig. 7. This likely nullifies some of the effects that the primary particle size distribution could have on the extinction spectrum or the photocatalytic activity. The particles were seen to sinter much less on soda-lime glass surface compared to the titania samples, which is clearly observable in Fig. S6. As the particles sinter, their shape change as well, which could potentially also change the plasmonic properties [34,35]. For some reason the sintering process on the surface varied significantly between the two substrates, even if all other parameters were kept identical. This is likely a major factor contributing in the disconnect between the VIS-Peak redshift observed in extinction spectrum and the photocatalytic activity. This hypothesis should be explored in future work by finding a solution to inhibit particle sintering on the surface. One option would be increasing the distance of the LFS burner from the substrate or possibly cooling the surface during deposition. Increasing the distance would, however, decrease the temperature gradient and therefore lower the deposition efficiency. It is also possible that the similar particle deposits behave plasmonically in a different way on the TiO_2 surface compared to soda-lime glass.

4. Conclusions

In this study, silver nanoparticles were produced with Liquid Flame Spray and deposited first on soda-lime glass slides (UV–Vis samples), and then on anatase TiO_2 thin film photocatalysts fabricated on quartz glass slides by Atomic Layer Deposition (photocatalytic activity samples). The UV–Vis samples were used to study how the extinction spectrum can be adjusted by tuning the LFS synthesis parameters, and the goal of coating the TiO_2 thin films was exploring the factors influencing their photocatalytic activity. These two perspectives together gave valuable insight for designing more efficient photocatalytic systems. The silver concentration in the precursor solution, the solvent composition, the precursor solution feed rate, the H_2 gas feed rate, and the number of coating cycles were the LFS parameters varied. In most sample sets, the theoretical silver loading on the surface was kept very similar among all samples in order to distinguish the differences caused by the structural design. An additional sample set was prepared with varying number coating cycles to study the effect of silver loading on the photocatalytic enhancement of the TiO_2 thin film.

The UV–Vis samples mostly expressed bimodal extinction spectra, one peak being centered in the UV region (UV-Peak) and the other in the visible light region (VIS-Peak). The position of the VIS-Peak was observed to correlate with the precursor solution feed rate and the silver mass concentration in the precursor solution. The peak redshifted as the concentration or the solution feed rate was increased. A simultaneous blueshift was observed for the UV-Peak. The primary particle sizes for each set of synthesis parameters were studied with TEM imaging, and the average particle sizes were calculated for particles over 5 nm in diameter that could be automatically measured from the micrographs. The redshift of the VIS-Peak was observed to correlate well with the increasing average particle size. As there always was a clear ultrafine particle mode ($d < 5$ nm) present that could be counted manually, the blueshift of the UV-Peak was attributed to the simultaneous decrease in the average size of the 0–10 nm fraction of the particles.

The photocatalytic activity of the samples was measured by acetylene photo-oxidation under high intensity broad spectrum light irradiation to see if the mentioned correlations could be coupled with photocatalytic enhancement of the TiO_2 thin film. Surprisingly, photocatalytic activity was not observed to correlate with the increase in particle size and the redshift of the VIS-Peak. Instead, the silver particle coverage of the TiO_2 surface seemed to be a more relevant factor for the photo-oxidation rate. The disconnect between the extinction spectrum and the photocatalytic activity is likely connected to the particle sintering on the titania surface compared to the soda-lime glass surface, thus changing the properties of the particle deposits measured for the soda-lime glass samples.

The samples were imaged with SEM to determine the silver coverages on the sample surfaces. The surface coverage values calculated with ImageJ correlated with the photocatalytic activity, when the surface coverage was roughly over 10 %. At first, adding silver raised the photoactivity, which peaked at around 30 % surface coverage, and then started to decrease. The initial increase in photocatalytic activity with growing silver loading was explained by plasmonic coupling of the silver particles with the TiO_2 explained by Temerov et al. [3] in more detail. The subsequent decrease was attributed to either silver particles blocking a significant portion of the active reaction area of the titania

surface or absorbing/scattering too large a fraction of the incoming light, decreasing the electron excitation in the TiO_2. The particles were also seen to agglomerate and sinter on the surface, especially when the number of coating cycles was clearly increased.

This study consisted of two parts, controlling the extinction spectra of silver nanoparticle coatings on soda-lime glass surface, and optimizing their photocatalytic enhancement on a TiO_2 surface. Even though the control of the extinction spectrum was not observed to correlate with the photocatalytic activity, there will likely be other areas of application where this type of control could be useful. Also, if the sintering behavior can be controlled better, a correlation could possibly be found. The effect of silver loading on the photocatalytic activity can be directly used for the upcoming studies, when moving to more complex surfaces of coatings. This gives a good basis for the next step of designing better photocatalytic systems. However, the effect of very low silver loadings of under 10 % surface coverage should still be explored as our samples could not adequately cover that.

CRediT authorship contribution statement

Miika Sorvali: Writing – review & editing, Writing – original draft, Visualization, Validation, Methodology, Investigation, Formal analysis, Data curation, Conceptualization. **Tuomas Tinus:** Writing – review & editing, Writing – original draft, Methodology. **Jerin Thamby:** Writing – review & editing, Validation, Methodology, Investigation, Formal analysis, Data curation. **Mari Honkanen:** Methodology, Formal analysis. **Harri Ali-Löytty:** Writing – review & editing, Investigation, Conceptualization. **Alireza Charmforoushan:** Writing – review & editing, Methodology. **Mika Valden:** Writing – review & editing, Supervision, Conceptualization. **Jarkko J. Saarinen:** Writing – review & editing, Supervision, Project administration, Investigation, Funding acquisition, Conceptualization. **Jyrki M. Mäkelä:** Writing – review & editing, Supervision, Project administration, Investigation, Funding acquisition, Conceptualization.

Declaration of competing interest

The authors declare that they have no known competing financial interests or personal relationships that could have appeared to influence the work reported in this paper.

Data availability

Data will be made available on request.

Acknowledgements

The authors want to acknowledge the Academy of Finland funding (nSTAR, Grant numbers 339544 and 339545). Academy of Finland Flagship for Photonics Research and Innovation (PREIN, decision no. 320166) is also acknowledged for support. The help of DSc. Matti Virkki and DSc. Suvi Lehtimäki is acknowledged in conducting the UV-Vis measurements. Miika Sorvali also wants to acknowledge Mr. Sami Mäkipää for his assistance with the sample preparation. The SEM and TEM imaging was performed at Tampere Microscopy Center facilities at Tampere University.

Appendix A. Supplementary data

Supplementary data to this article can be found online at https://doi.org/10.1016/j.matdes.2024.112800.

References

[1] X.L. Zhuo, X.Z. Zhu, Q. Li, J.F. Wang, Gold nanobipyramid-directed growth of length-variable silver nanorods with multipolar plasmon resonances, ACS Nano 9 (2015) 7523–7535.
[2] C. Peng, W. Wang, W. Zhang, Y. Liang, L. Zhuo, Surface plasmon-driven photoelectrochemical water splitting of TiO_2 nanowires decorated with Ag nanoparticles under visible light illumination, Appl. Surf. Sci 420 (2017) 286–295.
[3] F. Temerov, K. Pham, P. Juuti, J.M. Mäkelä, E.V. Grachova, S. Kumar, S. Eslava, J. J. Saarinen, Silver-decorated TiO_2 inverse opal structure for visible light-induced photocatalytic degradation of organic pollutants and hydrogen evolution, Appl. Mater. Interf. 12 (2020) 41200–41210.
[4] Y.-C. Pu, G. Wang, K.-D. Chang, Y. Ling, Y.-K. Lin, B.C. Fitzmorris, C.-M. Liu, X. Lu, Y. Tong, J.Z. Zhang, Y.-J. Hsu, Y. Li, Au nanostructure-decorated TiO2 nanowires exhibiting photoactivity across entire UV-visible region for photoelectrochemical water splitting, Nano Lett. 13 (2013) 3817–3823.
[5] M. Rycenga, C.M. Cobley, J. Zeng, W. Li, C.H. Moran, Q. Zhang, D. Qin, Y. Xia, Controlling the synthesis and assembly of silver nanostructures for plasmonic applications, Chem. Rev. 111 (2011) 3669–3712.
[6] Z. Wang, H. Sha, K. Yang, Y. Zhu, J. Zhang, Self-assembled monolayer silver nanoparticles: fano resonance and SERS application, Opt. Laser Technol. 157 (2023) 108771.
[7] Q. Chen, Y. Ye, J. Liu, S. Wu, P. Li, C. Liang, Stability evolution of ultrafine Ag nanoparticles prepared by laser ablation on liquids, J. Colloid. Interf. Sci. 585 (2021) 444–451.
[8] Z. Zuo, Y. Guo, J. Li, L. Zhang, Y. Feng, F. Liao, K. Li, G. Cui, Small-sized nanoparticle stacked films promoted by sustainedly released surfactants for plasmonic broadband super absorption, J. Alloys Comp. 935 (2023) 168148.
[9] P. Merkl, S. Zhou, A. Zaganiaris, M. Shahata, A. Eleftheraki, T. Therskleff, G. A. Sotiriou, Plasmonic coupling in silver nanoparticle aggregates and their polymer composite films for near-infrared photothermal biofilm eradication, ACS Appl. Nano Mater. 4 (2021) 5330–5339.
[10] G.A. Kelesidis, D. Gao, F.H.L. Starsich, S.E. Pratsinis, Light extinction by agglomerates of gold nanoparticles: a plasmon ruler for sub- 10 nm interparticle distances, Anal. Chem. 94 (2022) 5310–5316.
[11] B.D. Bhuskute, H. Ali-Löytty, M. Honkanen, T. Salminen, M. Valden, Influence of the photodeposition sequence on the photocatalytic activity of plasmonic ag-Au/TiO_2 nanocomposites, Nanoscale Adv. 4 (2022) 4335–4343.
[12] W.R. Erwin, H.F. Zarick, E.M. Talbart, R. Bardhan, Light trapping in mesoporous solar cells with plasmonic nanostructures, Energy Environ. Sci. 9 (2016) 1577–1601.
[13] D. Gogoi, A. Namdeo, A.K. Golder, N.R. Peela, Ag-doped TiO_2 photocatalysts with effective charge transfer for highly efficient hydrogen production through water splitting, Int. J. Hydrogen Energ. 45 (2020) 2729–2744.
[14] S.I. Mogal, V.G. Gandhi, M. Mishra, S. Tripathi, T. Shripathi, P.A. Joshi, D.O. Shah, Single-step synthesis of silver-doped titanium dioxide: influence of silver on structural, textural, and photocatalytic properties, Ind. Eng. Chem. Res. 53 (2014) 5749–5758.
[15] J.M. Mäkelä, H. Keskinen, T. Forsblom, J. Keskinen, Generation of metal and metal oxide nanoparticles by liquid flame spray, J. Mater. Sci. 39 (2004) 2783–2788.
[16] J.M. Mäkelä, J. Haapanen, J. Harra, P. Juuti, S. Kujanpää, Liquid flame spray – a hydrogen-oxygen flame based method for nanoparticle synthesis and functional nanocoatings, KONA Powder Part. J. 34 (2017) 141–154.
[17] M. Aromaa, H. Keskinen, J.M. Mäkelä, The effect of process parameters on the liquid flame spray generated titania nanoparticles, Biomol. Eng. 24 (2007) 543–548.
[18] M. Sorvali, M. Honkanen, L. Hyvärinen, R. Kuisma, J. Larjo, J.M. Mäkelä, Crystallographic phase formation of iron oxide particles produced from iron nitrate by liquid flame spray with a dual oxygen flow, Int. J. Ceramic Eng. Sci. 3 (2021) 227–236.
[19] J. Saari, H. Ali-Löytty, M.M. Kauppinen, M. Hannula, R. Khan, K. Lahtonen, L. Palmolahti, A. Tukiainen, H. Grönbeck, N.V. Tkachenko, M. Valden, Tunable Ti3+-mediated charge carrier dynamics of atomic layer deposition-grown amorphous TiO2, J. Phys. Chem. C 126 (2022) 4542–4554.
[20] R. Khan, H. Ali-Löytty, J. Saari, M. Valden, A. Tukiainen, K. Lahtonen, N. V. Tkachenko, Optimization of photogenerated charge carrier lifetimes in ALD grown TiO_2 for photonic applications, Nanomaterials 10 (2020) 1567.
[21] K. Pham, F. Temerov, J.J. Saarinen, Multicompound inverse opal structures with gold nanoparticles for visible light photocatalytic activity, Mater. Design 194 (2020) 108886.
[22] F. Temerov, B. Ankudze, J.J. Saarinen, TiO2 inverse opal structures with facile decoration of precious metal nanoparticles for enhanced photocatalytic activity, Mater. Chem. Phys. 242 (2020) 122471.
[23] D.D. Evanoff, G. Chumanov, Size-controlled synthesis of nanoparticles. 2. measurement of extinction, scattering, and absorption cross sections, J. Phys. Chem. B. 37 (2004) 13957–13962.
[24] A. Tricoli, T.D. Elmøe, Flame spray pyrolysis synthesis and aerosol deposition of nanoparticle films, AIChE J. 58 (2012) 3578–3588.
[25] E. Thimsen, P. Biswas, Nanostructured photoactive films synthesized by a flame aerosol reactor, Part. Technol. Fluid. 53 (2007) 1727–1735.
[26] L. Mädler, A. Roessler, S.E. Pratsinis, T. Sahm, A. Gurlo, N. Barsan, U. Weimar, Direct formation of highly porous gas-sensing films by in situ thermophoretic deposition of flame-made Pt/SnO_2 nanoparticles, Sensor. Actuat. B-Chem. 114 (2006) 283–295.

[27] K.B. Mogensen, K. Kneipp, Size-dependent shifts of plasmon resonance in silver nanoparticle films using controlled dissolution: monitoring the onset of surface screening effects, J. Phys. Chem. C 118 (2014) 28075–28083.
[28] S.K. Cushing, J. Li, J. Bright, B.T. Yost, B. Zheng, A.D. Bristow, N. Wu, Controlling plasmon-induced resonance energy transfer and hot electron injection processes in Metal@TiO_2 core-shell nanoparticles, J. Phys. Chem. C 119 (2015) 16239–16244.
[29] J. Li, S.K. Cushing, F. Meng, M.R. Senty, A.D. Bristow, N. Wu, Plasmon-induced resonance energy transfer for solar energy conversion, Nat. Photonics. 9 (2015) 601–607.
[30] S.N.G. Inturi, T. Boningari, M. Suidan, P.G. Smirniotis, Flame aerosol synthesized Cr incorporated TiO_2 for visible light photodegradation of gas phase acetonitrile, J. Phys. Chem. C 118 (2014) 231–242.
[31] S.N.G. Inturi, M. Suidan, P.G. Smirniotis, Influence of synthesis method on leaching of the Cr-TiO_2 catalyst for visible light liquid phase photocatalysis and their stability, Appl. Catal. B-Environ. 180 (2016) 351–361.
[32] B. Sun, E.P. Reddy, P.G. Smirniotis, TiO2-loaded Cr-modified molecular sieves for 4-chlorophenol photodegradation under visible light, J. Catal. 237 (2006) 314–321.
[33] C. Chambers, S.B. Stewart, B. Su, H.F. Jenkinson, J.R. Sandy, A.J. Ireland, Silver doped titanium dioxide nanoparticles as antimicrobial additives to dental polymers, Dent. Mater. 33 (2017) e115–e123.
[34] D. Li, R. Huang, X. Qian, C. Li, Preparation of triangular silver nanoplates by improved light-driven seed growth method, Inorg. Chem. Commun. 145 (2022) 110012.
[35] I.O. Sosa, C. Noguez, R.G. Barrera, Optical properties of metal nanoparticles with arbitrary shapes, J. Phys. Chem. B. 107 (2003) 6260–6275.